Metrology Research Institute

Angle-Resolved Measurements and Modelling of Diffuse Reflectance and Luminescence

Priit Jaanson

Aalto University

DOCTORAL DISSERTATIONS

Aalto University publication series
DOCTORAL DISSERTATIONS 195/2017
VTT SCIENCE 164

Angle-Resolved Measurements and Modelling of Diffuse Reflectance and Luminescence

Priit Jaanson

A doctoral dissertation completed for the degree of Doctor of Science (Technology) to be defended, with the permission of the Aalto University School of Electrical Engineering, at a public examination held at the lecture hall TU2 of the school on 3 November 2017 at 12.

Aalto University
School of Electrical Engineering
Metrology Research Institute

Supervising professor
Prof. Erkki Ikonen

Thesis advisor
Dr. Farshid Manoocheri

Preliminary examiners
Prof. Kai-Erik Peiponen, University of Eastern Finland
Dr. Li Yang, Innventia AB, Sweden

Opponent
Dr. Joanne Zwinkels, NRC, Canada

Aalto University publication series
DOCTORAL DISSERTATIONS 195/2017

VTT SCIENCE 164

ISBN 978-952-60-7657-7 (printed)
ISBN 978-952-60-7656-0 (pdf)
ISSN-L 1799-4934
ISSN 1799-4934 (printed)
ISSN 1799-4942 (pdf)
http://urn.fi/URN:ISBN:978-952-60-7656-0

ISBN 978-951-38-8575-5 (printed)
ISBN 978-951-38-8574-8 (pdf)
ISSN-L 2242-119X
ISSN 2242-119X (printed)
ISSN 2242-1203 (pdf)
http://urn.fi/URN:ISBN:978-951-38-8574-8

Unigrafia Oy
Helsinki 2017

Finland

NORDIC ECOLABEL
441 697
Printed matter

Aalto University

Abstract

Aalto University, P.O. Box 11000, FI-00076 Aalto www.aalto.fi

Author
Priit Jaanson

Name of the doctoral dissertation
Angle-Resolved Measurements and Modelling of Diffuse Reflectance and Luminescence

Publisher School of Electrical Engineering

Unit Metrology Research Institute

Series Aalto University publication series DOCTORAL DISSERTATIONS 195/2017

Field of research Optical Technology

Manuscript submitted 8 May 2017 **Date of the defence** 3 November 2017

Permission to publish granted (date) 28 July 2017 **Language** English

☐ **Monograph** ☒ **Article dissertation** ☐ **Essay dissertation**

Abstract

This thesis covers angle-resolved spectrophotometric measurements and modelling of diffuse reflectance and luminescence. Most of the work related to diffuse reflectance is performed in view of providing SI-traceability to radiative transfer codes used in Earth observation. The angle-resolved measurements of luminescent surfaces are used to study goniometrical properties of reflectance and luminescence of reference materials used in appearance measurements.

Radiative transfer models that simulate the transmission of light through atmosphere and vegetation are used to interpret the measurements of on-orbit sensors. One way of validating these models is using artificial targets that are characterised by SI-traceable measurements of reflectance and shape. The bidirectional reflectance factors of many roughened anodised and non-anodised surfaces were measured, and used to test the suitability of micro-facet scattering functions to present the scattering properties of such surfaces. Based on the results, a grooved and an identical flat target were constructed and characterised for bidirectional reflectance factors. The bidirectional reflectance factors of the flat target were used to parametrise the scattering functions for rough surfaces. The grooved target was measured for its coordinates describing shape, which were used to construct a structural model of the grooved target. The structural model, with its optical properties defined by the parametrised scattering functions, was used to simulate the bidirectional reflectance factors of the grooved target with the tested radiative transfer model. The measured and modelled bidirectional reflectance factors agreed within corresponding expanded uncertainties for most of the measured geometries, but not all.

Non-Lambertian emission of luminescence from solid luminescent materials has been established, however, instrumentation for angle-resolved measurements of luminescence have not been readily available. The MIKES-Aalto goniofluorometer was extensively characterised to improve the accuracy of bispectral luminescent radiance factor measurements. In addition, a method for goniometrical measurements of quantum efficiency and quantum yield was validated against interlaboratory measurements. The improved measurement capability was used to describe absorbance dependent reflectance angular profiles in solid amorphous luminescent materials. In addition, a reference material for luminescence measurements was proposed and characterised. The new material showed more Lambertian angular luminescence emission and reflectance profiles than the conventionally used materials.

Keywords reflectance, luminescence, bidirectional reflectance distribution function, bidirectional reflectance factor, radiance factor, bispectral luminescent radiance factor, quantum efficiency

ISBN (printed) 978-952-60-7657-7 **ISBN (pdf)** 978-952-60-7656-0

ISSN-L 1799-4934 **ISSN (printed)** 1799-4934 **ISSN (pdf)** 1799-4942

Location of publisher Helsinki **Location of printing** Helsinki **Year** 2017

Pages 102 **urn** http://urn.fi/URN:ISBN:978-952-60-7656-0

Preface

The research work leading to this thesis was carried out during 2010-2017 at Metrology Research Institute, Aalto University, at VTT MIKES Metrology, and for a brief period at JRC, European Commission.

I express my deepest gratitude to my supervising professor Erkki Ikonen, who has given me the opportunity to pursue the doctoral degree and guided me throughout the process. I also thank my thesis advisor Farshid Manoocheri for all the fruitful discussions, and for guidance in the practical work.

I thank my colleagues at the MRI group, who have contributed to the results of this work by creating a supportive environment for science to blossom. Especially, Tomi Pulli, Jalmari Toivanen, Henrik Mäntynen and Aigar Vaigu, who have directly contributed to the progress made with this thesis. In addition, I thank all the co-authors of the articles included in this thesis, and all the project partners, whose valuable perspective has shaped the contents of this work.

I thank the EMRP program for funding the projects MetEOC and xDReflect, from which this thesis is mainly financed.

I express gratitude to my parents who have always supported me in pursuing science, and to my sister, whose occasional shipment of cookies has fuelled many late nights in the lab. I thank my friends with whom the majority of evenings have been spent by on- and off-campus socialising, in- and out-of-city misguided wanderings, roped and ropeless ascensions, and on-court pursuits and off-court celebrations.

Lastly, I am grateful to my partner-in-life, Alice, whose tremendous support, endless patience, and countless words of wisdom, have been invaluable.

Contents

List of publications

This thesis is based on the following original publications which are referred to in the text as I–IV. Publications I, III and IV are reproduced with kind permission from the publishers.

I P. Jaanson, F. Manoocheri, H. Mäntynen, M. Gergely, J.-L. Widlowski, and E. Ikonen, “Gonioreflectometric properties of metal surfaces,” *Metrologia*, vol. 51, no. 6, pp. S314–S318, 2014.

II P. Jaanson, A. Bialek, C. Greenwell, H. Mäntynen, J-L. Widlowski, F. Manoocheri, A. Lassila, N. Fox, and E. Ikonen, “Towards SI-traceability of a Monte Carlo radiative transfer model in the visible range,” *IEEE Trans. Geosci. Remote Sens.* (accepted for publication).

III P. Jaanson, F. Manoocheri, and E. Ikonen, “Goniometrical measurements of fluorescence quantum efficiency,” *Meas. Sci. Technol.*, vol. 27, no. 2, 025204, pp. 1-8, 2016.

IV P. Jaanson, T. Pulli, F. Manoocheri, and E. Ikonen, “A reference material with close to Lambertian reflectance and fluorescence emission profiles,” *Metrologia*, vol. 53, no. 6, pp. 1330–1338, 2016.

Author's contributions

Publication I: The author contributed to the customisation and automation of the measurement setup, performed the measurements, and analysed the results.

Publication II: The author developed the algorithm for model parameter retrieval, performed the uncertainty analysis, modelling, and final analysis of the results.

Publication III: The author contributed to the automation of the measurement setup, did extensive characterisation of the goniofluorometer, developed procedures for data analysis, carried out the measurements, and analysed the data and the uncertainty of the measurement results.

Publication IV: The author performed the measurements and analysed the results.

The author wrote first versions of all the manuscripts and revised the texts based on the comments by the co-authors.

List of abbreviations

BRDF	bidirectional reflectance distribution function
BRF	bidirectional reflectance factor
CIE	International Commission on Illumination (*Commission Internationale de l'Eclairage*)
IZA	illumination zenith angle
MC	Monte Carlo
MIKES	Mittatekniikan Keskus
NMI	National Metrology Institute
OPD	orientation probability distribution
PRD	perfect reflecting diffuser
PTFE	polytetrafluoroethylene
RT	radiative transfer
SHD	surface height distribution
SI	international system of units
VZA	viewing zenith angle

List of symbols

A_s	shadowing function
d	nominal distance between the illuminated spot on the sample and the detector aperture
D	Lambertian BRF component
d^*	actual distance between the illuminated spot on the sample and the detector aperture
d_x	component of d in x direction
d_x^*	component of d^* in x direction
d_y	component of d in y direction
d_y^*	component of d^* in y direction
E	incident irradiance
f	bidirectional reflectance distribution function
k	coverage factor for 95% probability
L	radiance
$M_{\chi 00}$	Mueller matrix for describing the specular reflectance for polarisation χ
n	real part of the complex refractive index
R	weight of the specular BRF component
r_1	relative weight of the micro-facet orientation probability with σ_{m1}
$R_{L\lambda}$	hemispherical bispectral luminescent reflectance factor
T	micro-facet orientation probability distribution
x	coordinate along the horizontal axis
y	coordinate along the vertical axis
α	angle between the irradiating beam and the viewing direction of the detector
$\beta_{L\lambda}$	bispectral luminescent radiance factor
β_R	reflected radiance factor
Δx	displacement in x direction
Δy	displacement in y direction

$\Delta\theta_v$	displacement in the viewing zenith angle
$\Delta\lambda$	shift in the wavelength setting of the emission monochromator
η_L	quantum efficiency of luminescence process
θ_i	illumination zenith angle
θ_v	viewing zenith angle
θ_v^*	erroneous viewing angle
κ	imaginary part of the complex refractive index
λ	emission wavelength
λ_1, λ_2	emission range of a sample
λ_{max}	peak emission wavelength
μ	excitation wavelength
μ_{max}	peak excitation wavelength
ρ	bidirectional reflectance factor
σ_{m1}, σ_{m2}	root-mean-squared slopes of micro-facets
Φ_i	incident radiant flux
ϕ_i	illumination azimuth angle
Φ_r	reflected radiant flux
ϕ_v	viewing azimuth angle
Φ_r^*	erroneous reflected radiant flux
χ	polarisation (s or p)
Ω_v	solid angle of viewing

1. Introduction

1.1 Background

This thesis is about high accuracy angle-resolved spectrophotometric measurements. Spectrophotometry is the quantitative measurement of the interaction of ultraviolet, visible and infrared radiation with a material [1]. Spectrophotometric measurements of spectral reflectance, transmittance, absorbance, luminescence emission, scattering and other parameters are used in various industrial fields and scientific disciplines. The aim of this thesis is to reduce the uncertainties in angle-resolved spectrophotometric measurements and study the angular behaviour of reflectance and luminescence of materials.

Angle-resolved measurements of reflectance are used in describing the visual appearance of surfaces [2] (especially of goniochromatic coatings [3]), describing surface structures [4], measuring the thickness of thin layers [5,6] etc. In addition, satellite based Earth observation using on-orbit radiometers in the visible and near infrared range is essentially spectrophotometric measurement of reflectance of the surface of the Earth. The light from Sun is transferred through the atmosphere of Earth, is scattered from the Earth's surface and vegetation, and is transferred through the atmosphere again, before reaching the detector on the satellite. In order to interpret the measured values, the scattering in the atmosphere and in the vegetation needs to be taken into account by radiative transfer models such as the one [7] used for the moderate-resolution imaging spectroradiometer MODIS [8]. Consequently, the quality of the measurement results relies heavily on the quality of these models. The quality of radiative transfer models is usually determined by comparisons against field data [9] or other models [10] or by checking models' internal consistencies analytically [11]. Another way to validate these models is using artificial targets that comprise many individual surfaces whose scattering properties can be measured [12]. Determining the scattering properties of these surfaces relies on accurate angle-resolved diffuse reflectance measurements and physics based models that parametrise the scattering properties. With the parameters and structure of the artificial target, its overall reflectance can be simulated by the radiative transfer models and compared against laboratory-measured values.

Ever since the celestial blue glow of a quinine solution in the sunlight was reported for the first time [13], luminescent molecules – luminophores – have been used in different fields of science and industry. In medicine and biology, fluorescent markers are used to detect reactions that would otherwise go unnoticed [14], and with fluorescence microscopy, objects in the sizes below the diffraction limit can be viewed [15]. In industry, luminophores are used to enhance the colours of materials e.g. in paper industry fluorophores emitting blue light are used to make paper appear whiter [16], and luminescent dyes used in textiles and safety signs make the colours more vibrant and noticeable [17]. With luminescent pigments widely used in all these industrial fields, accurate colorimetric measurements of appearance and

quantum efficiency of luminophores are needed to dose the luminophores efficiently. Accurate measurements of quantum efficiency leading to accurate dosing of the luminophores may lead to significant savings in the multi-billion-euro pigment industry. The colorimetric measurements are usually performed at single geometry conditions in comparison to previously calibrated reference material [2], and luminescence emission is assumed Lambertian – having uniform radiance in all directions [18]. In contrary, it has been shown in [19,20] as well as in Publications III and IV, that luminescence emission from solid amorphous materials has non-Lambertian characteristics. Thus, assumptions in the angular luminescence emission profiles can lead to measurement errors. One option to avoid such errors is to measure luminescence emission goniometrically. The other is to provide reference materials that have more Lambertian properties than the conventional reference materials.

1.2 Thesis outline

In this thesis, the abovementioned issues are addressed. Angle-resolved diffuse reflectance of surfaces is measured and modelled with the goal of establishing SI-traceability of radiative transfer (RT) codes. The goniometrical measurement setup for luminescence emission [21] is improved to measure angle-resolved bispectral luminescent radiance factors at state of the art uncertainties. A reference material is proposed that exhibits more Lambertian emission of luminescence than conventionally used reference samples.

Chapter 2 covers validation of a Monte-Carlo (MC) ray tracing radiative transfer model through high accuracy measurements of angle-resolved diffuse reflectance. In addition, geometrical errors in the angle-resolved measurements are quantified. The susceptibility of angle-resolved reflectance measurements to geometrical errors is usually emphasized in literature (e.g in [22–24]), but not discussed quantitatively. Furthermore, the polarisation of reflected light from highly diffuse samples is discussed and used to parametrise physics based scattering models.

In chapter 3, a facility for goniometrical measurements of bispectral luminescent radiance factors is characterised and validated against interlaboratory measurements of luminescence quantum efficiency. In addition, a reference material is proposed that shows more Lambertian reflectance and luminescence emission than conventional polytetrafluoroethylene (PTFE) based materials. The thesis is summarised in chapter 4.

1.3 Scientific contribution

This thesis contains the following novel scientific results.

Publication I. The bidirectional reflectance distribution function (BRDF) of anodised and non-anodised roughened aluminium surfaces are measured at numerous illumination and viewing geometries. The BRDF measurement results are used to solve inverse problems of two micro-facet models in order to evaluate the suitability of the models to represent the reflective properties of these surfaces. It is found that

both of the models fit better to the BRDF measurement results of the non-anodised aluminium surfaces.

Publication II. A step towards rigorous SI-traceability of radiative transfer models is taken. A 3-D Monte-Carlo ray-tracing radiative transfer model is tested for its ability to simulate the bidirectional reflectance factors of a non-anodised aluminium target. The radiative transfer model uses the optical properties and the topographic structure of the target, which have been previously determined via SI-traceable measurements of coordinates and reflectance. The simulated and measured bidirectional reflectance factor (BRF) values agree within the corresponding expanded uncertainties for most of the measured geometries, but not all. For improved results, better measurements and modelling of the surface roughness and more consistent roughening process are needed.

Publication III. Thorough characterisation of MIKES-Aalto goniofluorometer is presented. Consequently, the accuracy of measuring bispectral luminescent radiance factors of solid flat materials is improved. The improved measurement capability is applied to confirm the non-Lambertian emission of luminescence from solid amorphous materials. In addition, a previously proposed method for goniometrical measurements of fluorescence quantum efficiency and quantum yield is experimentally confirmed and validated through one of the first interlaboratory inter-instrumental measurements of this kind.

Publication IV. A reference material is presented showing more Lambertian angular luminescence emission and reflectance than conventional PTFE based materials. In addition, spectrally dependent angular reflectance profiles from commercially available luminescent diffuse reflectance reference materials are reported. The spectrally varying angular reflectance profiles are explained qualitatively and quantitatively by models. It is concluded that the spectral variation of angular reflectance profiles is caused by the absorbance of the luminophores and the volume scattering in the samples. The new reference material displays smaller spectral variation in angular reflectance profiles than PTFE.

2. Angle-resolved diffuse reflectance

Reflectance is defined as the ratio of reflected radiant flux to incident radiant flux [25]. In this thesis, reflectance is considered more specifically in terms of radiant flux of the light that is elastically scattered into the hemisphere that is limited by the surface of the sample and includes the direction of illumination. The angular distribution of reflected radiant flux depends on the material. A perfect mirror reflects all the incident light in a single direction according to the law of reflection [26] as visualised in Figure 1 on the left. A Lambertian diffuser is a surface that scatters all the incident light over the hemisphere with a uniform radiance in all directions as visualised in Figure 1 in the middle. The reflectance of all real surfaces, however, is less than one, and the angular distribution of reflected radiance deviates from both of the extreme cases described above. An example of an arbitrary angular distribution of reflected light is visualised in Figure 1 on the right.

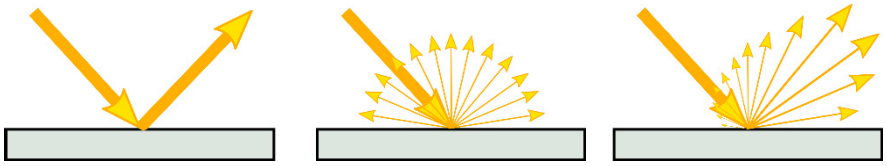

Figure 1. Types of reflectance: specular reflectance of a perfect mirror, diffuse reflectance of a Lambertian diffuser, arbitrary angular reflectance distribution that could be observed on a real surface.

2.1 Definitions of BRDF and BRF

The angular distribution of reflected light from a surface is described by the bidirectional reflectance distribution function (BRDF). BRDF for a uniformly irradiated surface is the ratio of the scattered radiance L to the incident irradiance E [22]

$$f(\theta_i,\phi_i,\theta_v,\phi_v)=\frac{L(\theta_v,\phi_v)}{E(\theta_i,\phi_i)}. \tag{1}$$

The angles θ_i and ϕ_i (θ_v and ϕ_v) are the illumination (viewing) zenith and azimuth angles. Generally, a small illumination spot is used and the BRDF is practically calculated as

$$f(\theta_i,\phi_i,\theta_v,\phi_v)=\frac{\Phi_r(\theta_v,\phi_v)}{\Phi_i(\theta_i,\phi_i)\Omega_v\cos\theta_v}, \tag{2}$$

where Φ_i is the radiant flux incident on the sample and Φ_r is the radiant flux reflected from the sample into a solid angle of Ω_v , as seen in Figure 2.

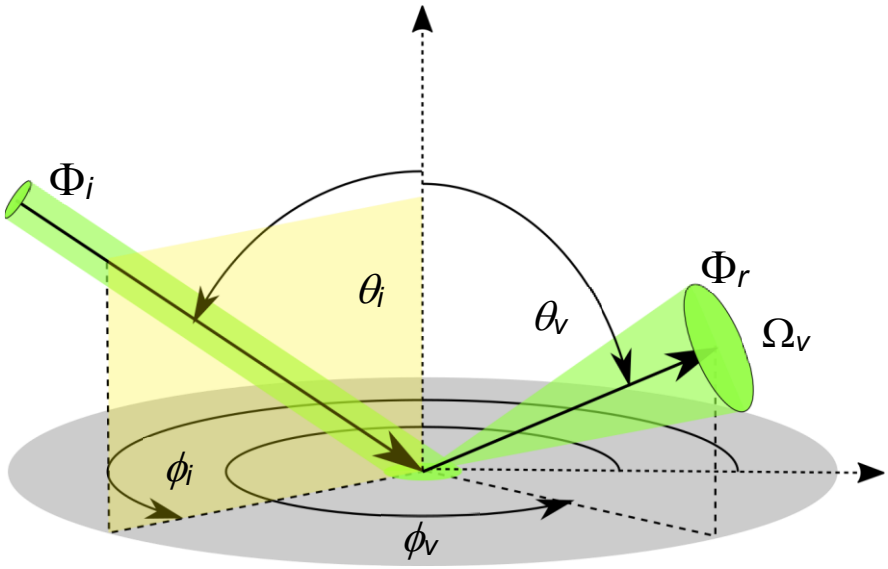

Figure 2. Geometry of BRDF. The polarisation state of the measured radiant flux Φ_r is defined by the polarisation direction of the incident light – s when perpendicular and p when parallel to the plane of incidence (shaded yellow), defined by the illumination direction and the surface normal.

Another widely used quantity in describing the angular distribution of reflected light is the bidirectional reflectance factor (BRF). BRF is defined as radiant flux reflected from a surface to a given solid angle divided by the reflected flux from a perfect reflecting diffuser (PRD), identically illuminated and viewed [27]. In the case of unidirectional irradiance, the BRF is

$$\rho = \pi f . \tag{3}$$

When the solid angle of viewing approaches zero, the reflectance factor is equal to the reflected radiance factor β_R.

2.2 Measurements of BRF

Recent decades have witnessed a rise in the demand for accurate BRF measurements of surfaces, resulting in development of goniospectrophotometers in many National Metrology Institutes (NMIs). The developed instruments differ from each other, however they fall generally in two categories in how the viewing and illumination geometries are realised. Some setups make use of a robotic arm as a sample holder such as the one in [28]; the others make use of stacked linear and rotary stages such as the measurement setup used in this work [29].

Many European research projects have been funded to improve the accuracy of BRF measurements to satisfy the needs of industry e.g. [30] and Earth observation community e.g. [31]. The current state of the art expanded uncertainties (k = 2) in

measuring the BRF of white reference samples at single geometry conditions is well within 0.5% [32].

In practice, measurements of BRF are conducted by measuring the ratio of reflected radiant flux to incident radiant flux at intended geometric conditions and thereafter the geometry factor is applied. The main sources of error in the measurements are related to the stray light caused by the beam guiding optics [33], the degree of polarisation of the reflected light, and the illumination and viewing geometries influenced by the alignment of the setup and the sample under measurement. The latter two can be many times larger than the other components if unaccounted.

2.2.1 Sample alignment errors in BRF measurements

Given the illumination and viewing geometries involved in goniometrical measurements of BRFs, the importance of accurate alignment of the setup and the sample within the setup cannot be emphasized enough. The alignment of the goniometrical measurement setup is usually performed by narrow beam alignment lasers and with the help of specular reflection from front surface mirrors. However, with diffusely reflecting samples, the alignment methods making use of specular reflection require the use of an alignment mirror. The alignment mirror then needs to be either brought to contact with the front surface of the sample through a lens cleaning paper or the sample holder needs to be in contact with the front surface of the sample, so the change of samples would not cause a change in alignment. However, contact with the front surface of the sample may be undesirable due to the risk of sample contamination and deformation. Other options include a telescopic camera system [34] or a stereo camera and a line projector. The latter two avoid contact with the front surface of the sample and are accurate, but can be difficult to adopt, especially to a commercial goniospectrophotometer.

In the following paragraphs, three scenarios of misalignment are discussed. The effects of misalignment on the measured reflected radiant flux are quantified for the specific case of MIKES-Aalto gonioreflectometer [29] assuming a perfect reflecting diffuser as a sample and a small irradiated area. It can be seen by finding the partial derivative of Eq. (2) with respect to Φ_r that the relative error in the measured radiant flux is equal to the relative error in the BRDF and BRF. Similarly, these geometric considerations affect the measurements of luminescence emission discussed in section 3.

The geometry of the MIKES-Aalto gonioreflectometer is shown in Figure 3. In a perfectly aligned measurement setup, the front surface of the sample is located on its axis of rotation (red dot in Figure 3). The rotation axis of the detector aperture A (black circle in Figure 3) coincides with the sample rotation axis. The illuminating beam of light (yellow arrow in Figure 3) crosses and is perpendicular to the abovementioned axes of rotation.

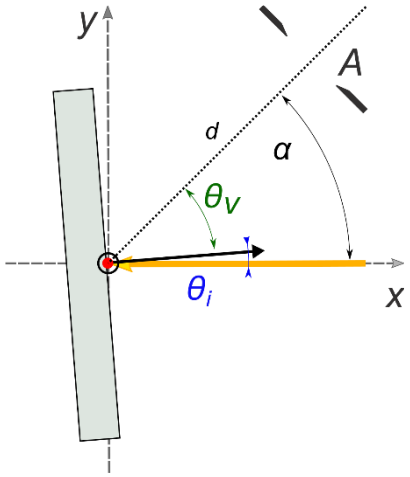

Figure 3. The geometry of a perfectly aligned MIKES-Aalto gonioreflectometer. The symbol α is the angle between the illuminating beam and the viewing direction of the detector and d is the distance from the illuminated spot on the sample to the detector aperture.

The measured quantity in BRF measurements, the reflected radiant flux Φ_r, can be expressed from Eq. (2) as

$$\Phi_r = f\Phi_i\Omega_v \cos\theta_v. \tag{4}$$

The solid angle Ω_v can be calculated as

$$\Omega_v(d) = \frac{\pi r^2}{d^2 + r^2}, \tag{5}$$

where r is the radius of the circular aperture of the detector and d is the distance from the sample to detector aperture. In MIKES-Aalto gonioreflectometer, d = 471.15 mm and r = 12.498 mm.

Scenario 1. The simplest to evaluate, yet having the largest effect on the measured value is the error in the viewing zenith angle (VZA) $\Delta\theta_v$. Differentiating Eq. (4) with respect to θ_v, gives a relative change in Φ_r as $\Delta\theta_v \tan\theta_v$, [24].

Scenario 2. The front surface of the sample is displaced by Δx from the rotation axes as shown in Figure 4. This error is introduced when the sample is replaced between alignment and measurement. For example, a mirror is used for alignment and then replaced with the sample under measurement, or an alignment mirror is used in contact with the sample as described above.

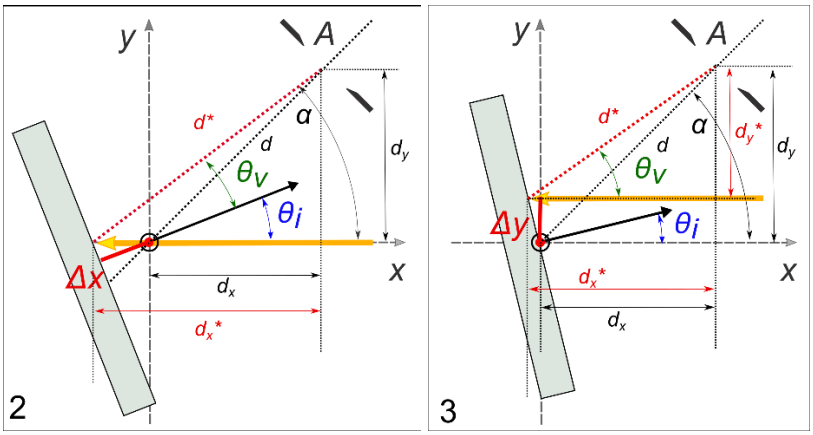

Figure 4. Geometries of misalignment. Scenario 2: the sample is displaced by *Δx* from the axes of rotation in *x* direction. Scenario 3: the illuminating beam is displaced from the axes of rotation by *Δy* in *y* direction.

The measured reflected radiant flux in this case is

$$\Phi_r^* = f\Phi_i \frac{\pi r^2}{d_x^{*2} + d_y^{*2} + r^2} \cos\theta_v^* , \tag{6}$$

where

$$d_x^* = d\cos\alpha - \frac{\Delta x}{\cos\theta_i} ,$$

$$d_y^* = d\sin\alpha , \quad \text{and}$$

$$\theta_v^* = \tan^{-1}\left(\frac{d_y^*}{d_x^*}\right) - \alpha .$$

The relative error in the measured reflected radiant flux is evaluated for several geometries and displacements in Figure 5. It can be seen that the relative error is negligible when Δ*x* is small (0.1 mm), however, with positioning error of 1 mm, the error in the measured value can be more than 0.5%.

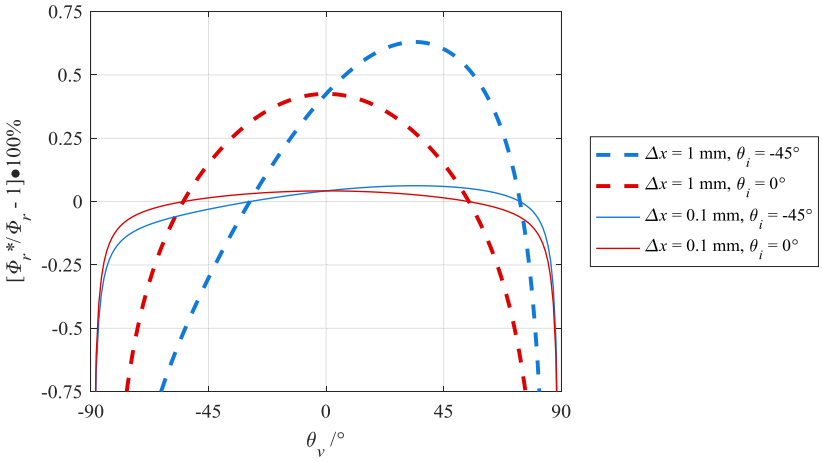

Figure 5. Relative error in the measured reflected radiant flux when the surface of the sample is displaced by Δx from its axis of rotation in an otherwise perfectly aligned setup.

Scenario 3. The illuminating beam is displaced from the axes of rotation by Δy as shown in Figure 4. This is effectively the case, when the irradiance on the sample is not uniform. The resulting measured reflected radiant flux can be again calculated with Eq. (6), where

$$d_x^* = d\cos\alpha - \Delta y \tan\theta_i \quad \text{and}$$
$$d_y^* = d\sin\alpha - \Delta y\,.$$

The relative error in the measured reflected radiant flux is evaluated for several geometries and displacements in Figure 6. It can be seen that the relative error is negligible when Δy is small (0.1 mm), however, with positioning error of 1 mm, the error in the measured value can be more than 0.5%.

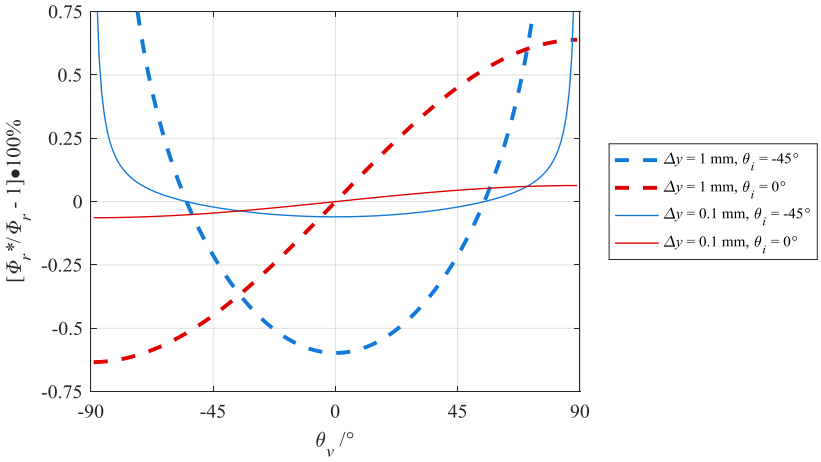

Figure 6. Relative error in the measured reflected radiant flux when the illuminating beam is displaced by *Δy* from the axis of rotation of the sample in an otherwise perfectly aligned setup.

2.2.2 Polarisation resolved measurements of BRFs

In Publication I, it was shown that BRDF of anodised and non-anodised roughened metal surfaces is highly dependent on the polarisation of the incident light. The BRFs of similar anodised and non-anodised surfaces with different illumination zenith angles (IZA) are shown in Figure 7. It can be seen that for these metallic surfaces, the differences in the polarised BRF values are small when the IZA is 0°. However, as the IZA increases the differences in the measured polarised BRFs increase, reaching up to a factor of 2 for non-anodised aluminium and a factor of 10 for anodised aluminium at IZA of -60°. Such behaviour is expected since these surfaces are not perfect diffusers and exhibit a specular component. The specularly reflected light, that can be described by the Fresnel formulae [26], has been shown to be less polarised for aluminium [35] than for aluminium oxide [36].

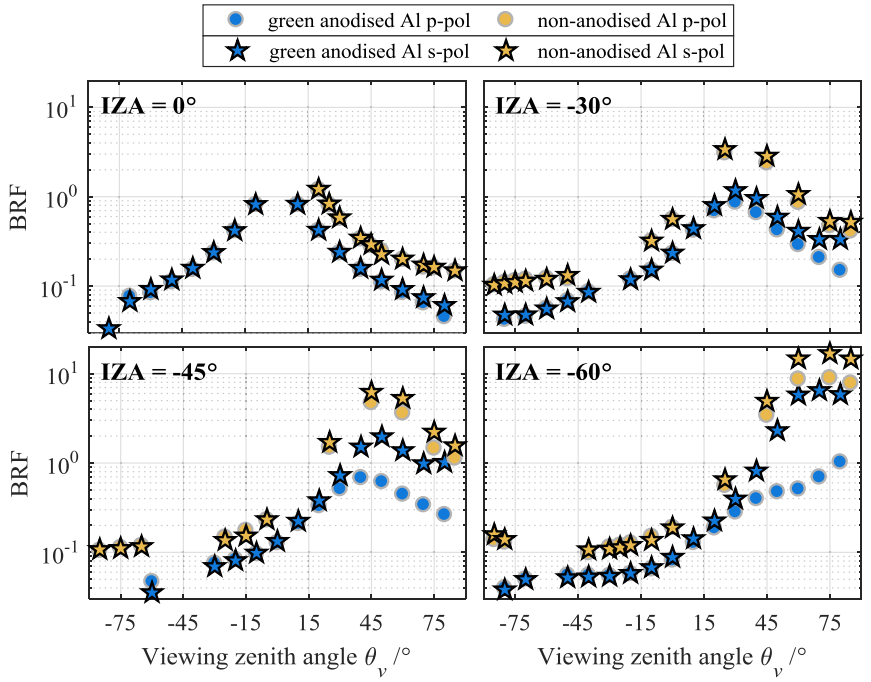

Figure 7. BRFs of anodised and non-anodised aluminium for different illumination zenith angles at the wavelength of 525 nm.

Similar effects can be seen in the measured polarisation resolved BRF values of materials that are generally regarded as nearly PRDs as shown in Figure 8. These materials, such as sintered and pressed PTFE and porous quartz, are used as reference materials for diffuse reflectance measurements. The differences between the corresponding polarised BRF values are much smaller for these surfaces than for the metallic surfaces shown in Figure 7.

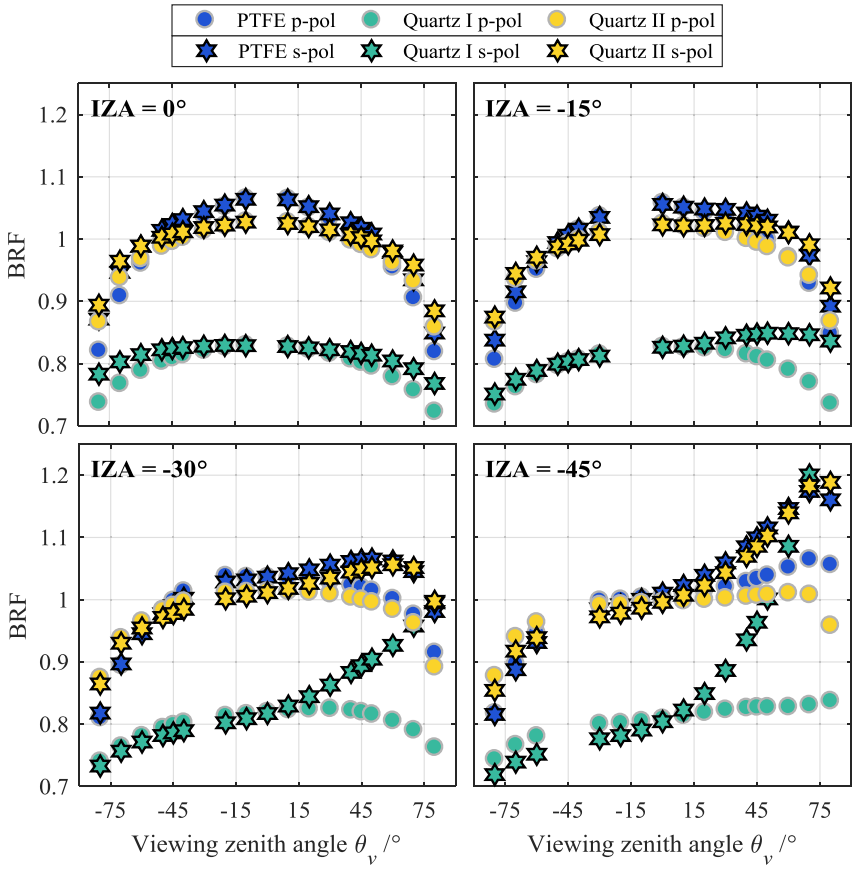

Figure 8. In-plane BRF measured with polarised incident light at the wavelength of 525 nm.

Many goniospectrophotometers illuminate the sample with monochromatic light. The monochromator and the beam guiding optics polarise the illuminating light. Thus, in order to obtain reliable measurements of the BRFs, it is important to introduce a depolariser or control the polarisation of the illuminating beam of light. Polarisation resolved measurements of angle-resolved diffuse reflectance make the already time costly measurement procedure even more so. However, the polarisation resolved BRF data provide useful information for parametrisation of BRDF models, which is required for validation of radiative transfer models as described below.

2.3 SI-traceable validation of radiative transfer models

Satellite based measurements provide an important source of information to quantify and monitor geophysical processes. The interpretation of the measured data

relies heavily on the quality of radiative transfer (RT) models that are used to simulate the radiation transfer in complex terrestrial environments e.g. atmosphere, soil and tree canopies. The validation of canopy RT models has so far relied on comparisons to in situ measurement data as was done in [9] and comparisons to other RT models as in [11]. The former suffers from the uncertainties of measuring the complexities of natural environments, the latter, while excellent in establishing the credibility of models, can never be an SI-traceable validation approach, due to the lack of comparable measurement results.

In Publication II, another option for validating the performance of a Monte-Carlo ray tracing RT model [12] is shown. The method, first presented in [12] and explained by the diagram in Figure 9, relies on accurate laboratory measurements of the BRFs and an accurate structural model of an artificial target. In the validation scheme, two targets of similar material and surface roughness are used, with the exception that one has a structured surface and the other is flat. The BRF measurement results of the flat target are used to parametrise a BRDF model as described in more detail in section 2.3.1. The coordinate measurements of the grooved target are used to create a structural model of the target to be used in the RT model, as described in more detail in section 2.3.2. The parameters and the structural model of the target are used to simulate the BRFs of the grooved target with the RT model and compared against the SI-traceable laboratory measured BRF values.

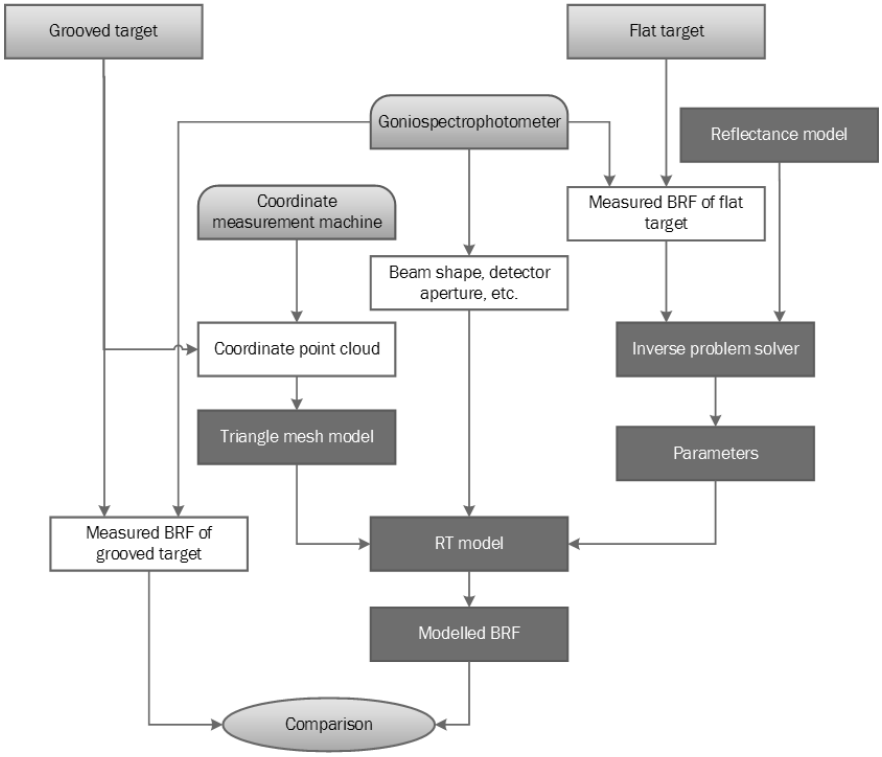

Figure 9. Diagram for SI traceable validation of the RT model.

The validation scheme, presented above, is not complete, because it provides information only for the tested conditions. In fact, a simulation tool can never be validated completely, because there will always be at least one more scenario, that was not tested [37]. However, with sufficient available data, models could be validated in most of the scenarios they are used in and thus the scheme described above is a useful step towards the SI-traceable validation of RT models.

Validation of radiative transfer models requires an accurate virtual replica of the target, and a reference data set that is suitable to evaluate the quality of the RT model simulations. Next two sections cover the construction of the virtual replica of the grooved target.

2.3.1 Micro-facet BRDF model and inverse problem solving

The RT model, used in this thesis, relies on sub-models that describe the probability of the scattering directions of rays upon colliding with a surface. There are many available models that describe the scattering of light from surfaces, ranging from empirical models (e.g. [38]) to analytical wave-optics based (e.g. [39]) models to statistical geometric optics based models (e.g. [40]).

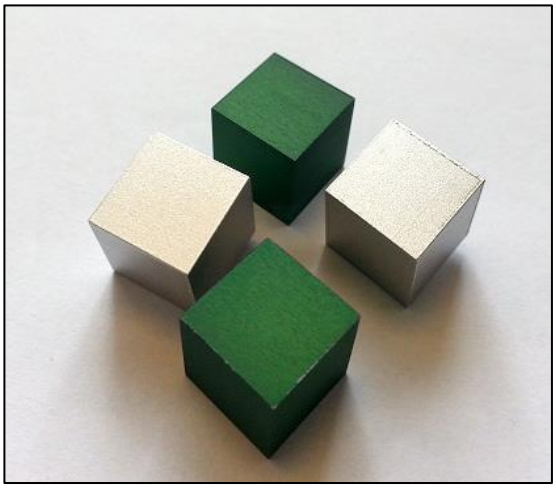

Figure 10. Anodised and non-anodised roughened aluminium surfaces. The dimensions of the cubes are 12 mm x 12 mm x 12 mm. In order to avoid the edges from rounding, the roughening process was performed for multiple samples at once, with the sides of the cubes tightly adjacent to each other.

In Publication I, a set of anodised and non-anodised aluminium surfaces, shown in Figure 10, were measured for their surface roughness. It was determined that the micro-facet models based on the Torrance-Sparrow formulation [41], describing the scattering of light from rough surfaces through geometrical optics, are suitable for this work. Thereafter, the BRFs of these surfaces were measured and used to find parameters for two micro-facet models: the Torrance-Sparrow formulation [41] and the energetically bound polarised micro-facet model adapted from [42] and [43]. It was determined, that 1) both models describe the BRFs of non-anodised surfaces better than the BRFs of anodised surfaces, 2) the polarised model and the availability of polarised measurements improve the parameter retrieval process, 3) neither of the models can describe the BRFs of the surfaces at all viewing and illumination geometries.

As a result, in Publication II, a polarised BRDF model with a more sophisticated micro-facet orientation probability distribution (OPD) and a simpler diffuse component was adapted. More specifically, the altered version of the Torrance-Sparrow micro-facet model describes the BRF of a surface as:

$$\rho_{\chi}(\theta_i,\phi_i,\theta_v,\phi_v) = D + R\left[r_1 T(\sigma_{m_1}) + (1-r_1)T(\sigma_{m_2})\right]\frac{M_{\chi_{00}}(n,\kappa)A_s}{4\cos(\theta_i)\cos(\theta_v)}, \qquad (7)$$

where χ stands for the polarisation of the incident radiation (either s or p relative to the plane of incidence), D is a constant diffuse BRF component and R is the weight of the specular BRF component. The expression in the brackets describes the micro-facet (OPD), where T is a micro-facet OPD resulting from Gaussian surface height distribution (SHD) adapted from [44], r_1 is the relative weight of the first OPD,

and σ_{m1} and σ_{m2} are the root-mean-squared slopes of the micro-facets. Parameter $M_{\chi 00}$ describes the Fresnel reflectance coefficients for χ-polarised incident radiation in the Mueller notation [45], A_s is the surface self-shadowing coefficient described in [46], and n and κ are the real and imaginary parts of the refractive index, respectively.

Finding the parameters for Eq. (7) requires solving an inverse problem, by finding the “best fit” of Eq. (7) to the measured BRF data. Inverse problems are difficult to solve for at least two reasons. First, many sets of model parameters may be consistent with the data. Secondly, to find the parameters, a large parameter space with dimensionality of the amount of parameters may need to be explored. The latter is simplified due to the model in Eq. (7) being physics based. Thus, the reasonable range for the complex refractive index can be estimated based on measured values of similar materials e.g. aluminium in [35]. Furthermore, the range for the root-mean-squared slope of the micro-facets can be estimated from the measured values of similarly processed materials from Publication I.

Initially the parameters D, R, σ_{m1}, σ_{m2}, r, n and κ were retrieved by fitting Eq. (7) to the measured BRF values of the targets. The fit was evaluated by the weighted sum of the squared residuals. The parameter search was performed using a genetic search algorithm *ga* in MATLAB to find the global optimum and thereafter the local optimum was found using a constrained nonlinear solver *fmincon* [47]. This way, however, the results of the fitting were highly dependent on the weights used. The reason can be seen in Figure 11. Even with the polarised measurements available, the model is over-defined by the parameters. In Figure 11, each column shows how the respective parameter influences the value of the function. The range, that the parameter is varied over, is specified with the colour bar on the top of the column. It can be seen that the parameters R, σ_{m1}, n and κ have a similar effects on the value of the function.

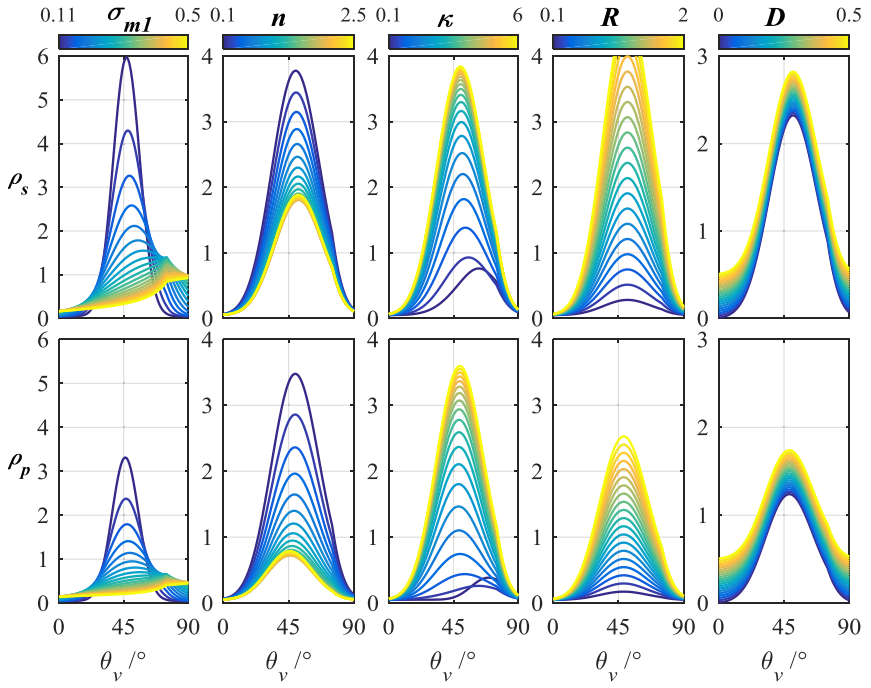

Figure 11. The BRF values ρ_s and ρ_p, calculated by Eq. (7), with r_1 = 1. The parameters σ_{m1}, n, κ, R and D are varied in columns 1-5, respectively. The function is evaluated for the illumination zenith angle θ_i= 45° and relative azimuth angle of 180°. All the subfigures have the function value (BRF) on the vertical axis and the VZA θ_v on the horizontal axis

Figure 12 shows that the ratio of s- and p-polarised BRF components is sensitive to n and κ, but less so for other parameters. Thus, in order to improve the parameter retrieval process, the ratio of polarised BRFs needs to be taken into account. Resulting cost function for the parameter retrieval takes into account the sum of the squared residuals between the measured and the modelled BRF values, the ratio of polarised BRF components, and the slope of the regression line for the scatterplot of measured and modelled BRFs. The resulting parameter values are presented in Publication II.

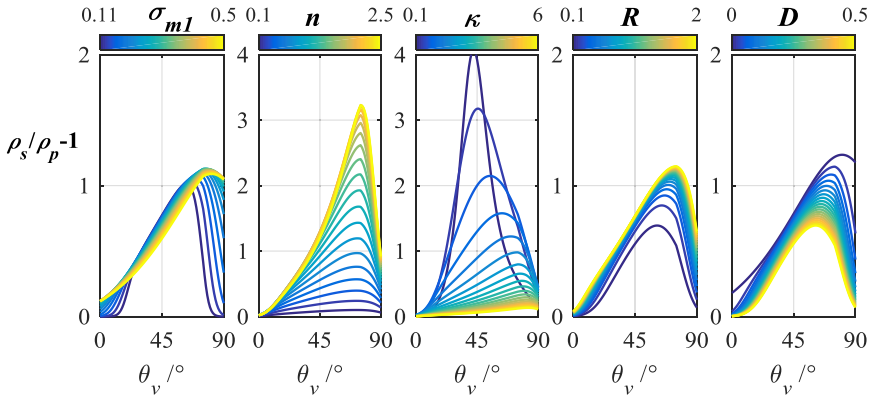

Figure 12. Polarisation of the modelled BRFs expressed by ρ_s/ρ_p-1, calculated by Eq. (7), with r_1 = 1. The parameters σ_{m1}, n, κ, R and D are varied in columns 1-5, respectively. The function is evaluated for the illumination zenith angle θ_i= 45° and relative azimuth angle of 180°. All the subfigures have the function value (BRF) on the vertical axis and the VZA θ_v on the horizontal axis.

2.3.2 Structural model of the target

As was emphasized in section 2.2.1, the geometric errors in the setup can lead to large uncertainties in the measured BRF values. Thus, in order to compare the measured and modelled BRF of the grooved target, high accuracy structural model is needed for the modelling.

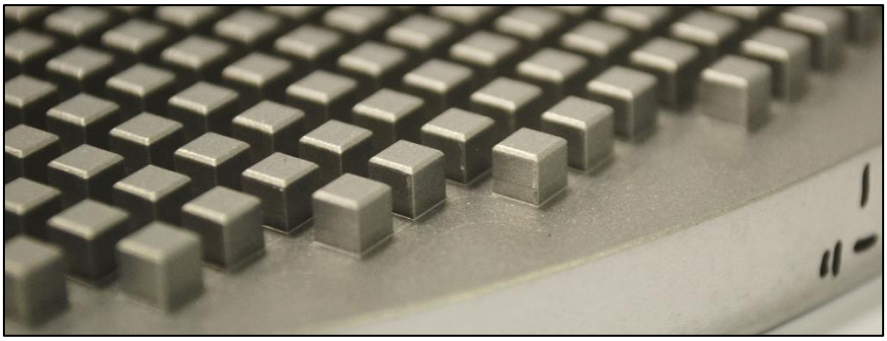

Figure 13. Photo of the grooved target. The edges of the cubes have become rounded in the roughening process.

The grooved target (shown in Figure 13) was measured for its coordinates with the coordinate measurement machine in MIKES [48]. In addition, the roundness of the edges of some of the individual cubes seen in Figure 13 was measured. The measured sets of coordinates were used to create a continuous structural model of

the target shown in Figure 14. The coordinate measurements, the process of creating the structural model, and the uncertainties of the structural model are presented in detail in publication II.

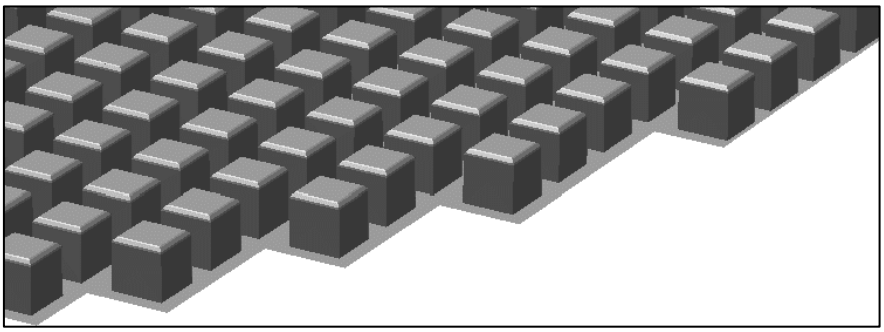

Figure 14. Structural model of the grooved target.

2.3.3 Comparison of measured and modelled BRF values

Two sets of parameters are found by solving the inverse problem of Eq. (7) with the measured BRF values of the flat target. One with r_1 set to 1, assuming a Gaussian SHD, the other describes the micro-facet OPD by two Gaussian SHDs. The resulting parameter values are presented in Table 1.

Table 1. Estimated parameter values for equation Eq. (7) retrieved from the BRF measurement results of the flat target (from Publication II). The values in parentheses indicate the standard uncertainty of the parameters.

Parameter	Value	
	RT1	*RT2*
n	1.0(1)	1.1(1)
κ	2.9(2)	3.0(2)
σ_{m1}	0.16(1)	0.16(1)
σ_{m2}	-	0.37(3)
R	2.5(2)	2.5(2)
D	0.14(3)	0.12(1)
r_1	1	0.6(1)

Next, the estimated parameter values and the structural model of the grooved target are used to simulate the BRFs of the grooved target with the RT model. A set of modelled and measured BRFs and the respective expanded uncertainties (k = 2)

are shown in Figure 15. The modelling uncertainty includes the uncertainty of the estimated parameters, the uncertainty associated with the geometry of the structural model of the grooved target as well as the uncertainty of positioning the actual grooved target within the measurement setup. The uncertainty of the estimated parameters is dominated by the expected differences in the scattering properties of the grooved and flat targets.

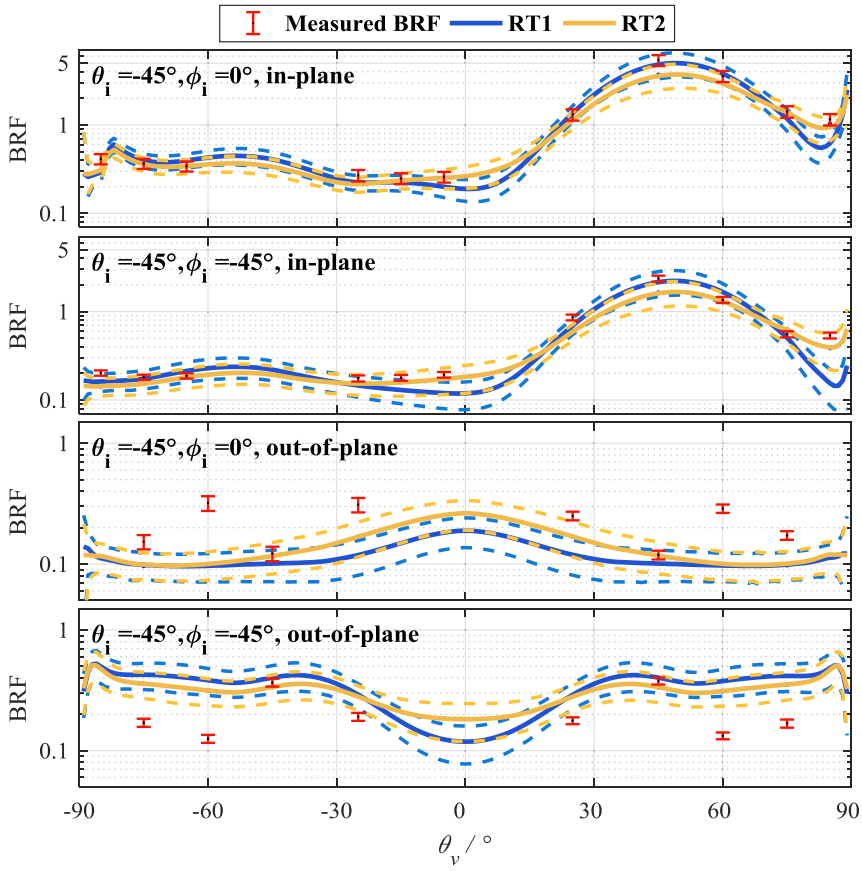

Figure 15. Measured and simulated BRF values. RT1 and RT2 are the modelling results for Gaussian and non-Gaussian SHDs, respectively. The uncertainty bars represent the expanded uncertainty (k = 2) of the measurement results. The dashed lines represent the expanded uncertainty (k = 2) of the modelling.

A detailed analysis of the results is presented in publication II. In summary, most of the measured and modelled values agreed within the corresponding expanded uncertainties. Out of the BRF values measured at 336 different geometries, the modelled BRF values agreed for 48% and 60% for parameter sets RT1 and RT2, respectively. However, since the uncertainties are expressed in a 95% confidence

level, the number of values in agreement is expected to be higher. The causes for the remaining observed BRF differences were identified as incomplete information about grooved target's surface roughness, and the inability of the Torrance-Sparrow formulation to describe the scattering properties of the flat target's surface under all illumination and viewing conditions.

The work done is a step towards SI-traceability of RT models. However, the full SI-traceability of MC RT models will have to be achieved through improved measurement facilities providing the data from which the structural and optical properties of real targets can be obtained. In order to improve the validation process, the cubes on the grooved target could be manufactured separately and roughened under better-controlled conditions with sides tightly adjacent to each other, as was done in Publication I. In addition, improved surface roughness measurements could be conducted from which the micro-facet orientation probability distribution can be determined without any assumptions, as discussed in Publication II.

3. Photoluminescence

Photoluminescence is a term used to describe a phenomenon in which light is absorbed by a molecule and subsequently re-emitted at longer wavelengths [49]. The energy of the absorbed photons excites the electrons in the luminescent molecule –the luminophore – into higher energy states. As the electrons relax back to the lower energy states, energy is released and photons are emitted as light [50]. The spectral range at which the photon energy is absorbed is referred to as the excitation range; and the spectral range at which the photons are emitted is referred to as the emission range.

Photoluminescence is a common name for two phenomena: fluorescence and phosphorescence. The difference between these two phenomena is the transition time: fluorescence occurs within 10 ns of excitation, phosphorescence lifetimes are generally between 1 ms and 1 s but in certain cases even more than that [50]. Fluorescence happens by electron relaxation from a singlet state to the ground state, phosphorescence happens by relaxation of electron from a triplet state to the ground state [50].

Photoluminescent molecules or luminophores are commonly used in different industries to enhance the colours of materials [17]. In paper industry, dyes that absorb radiation in the ultra-violet (UV) range of electromagnetic radiation and re-emit at blue wavelength range are used to make paper appear whiter [16]. In textile industry, fluorophores with various emission ranges are used to make the colours of fabrics appear more vibrant.

In this thesis, we concentrate on the steady state measurements of appearance of photoluminescent materials, as is the practice in the industries mentioned above. From this perspective, the distinction between fluorescence and phosphorescence is not essential; instead, both of the terms will be referred to as luminescence.

In Figure 16, a set of PTFE based luminescent diffuse reflectance reference materials is shown [51]. These materials are commonly used in industry as reference samples for colorimetry. The samples are excited with 380 nm light and emit at different ranges of visible light. As can be seen, the colour of each of the samples is different, and thus the colorimetric appearance of these samples depends on both the spectral reflectance and the spectral emittance of luminescence.

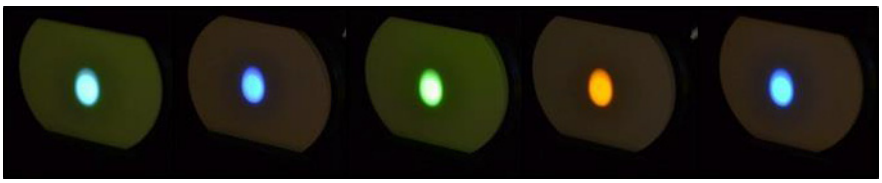

Figure 16. A set of PTFE based photoluminescent materials illuminated at the wavelength of 380 nm in the MIKES-Aalto goniofluorometer.

In the industry, the colorimetric measurements are usually performed at single geometry conditions in comparison to previously calibrated reference materials [2], and luminescence emission is assumed to be Lambertian. However, as it has been shown in [19,20] as well as in Publications III and IV, luminescence emission from commercially available luminescent diffuse reflectance reference materials deviates from Lambertian. Thus, assumptions in the angular luminescence emission profiles can lead to measurement errors. Options to avoid such errors are measuring luminescence emission goniometrically, or providing reference materials that have more Lambertian characteristics than the conventional reference materials. Both of these options are discussed below.

3.1 Background and methods

The methods for measuring diffuse reflectance of non-luminescent surfaces are inadequate for luminescent surfaces, since the amount of luminescence in the radiance spectrum of the surface depends on the spectral composition of incident light.

The methods for measuring the appearance of luminescent materials are generally divided into two categories based on the number of monochromators used: one or two. The methods based on one monochromator rely on adjusting the spectral irradiance on the luminescent sample by filters or other means and separating the luminescent and reflected components by computation (e.g. [52]). The two-monochromator method, considered as the reference method for determining the appearance of luminescent materials, is the most accurate and employs one monochromator –the excitation monochromator - for irradiation and another monochromator – the emission monochromator – for viewing. The wavelength settings of the excitation monochromator and the emission monochromator are usually noted by variables μ and λ, respectively.

In order to describe the appearance of luminescent materials, two concepts are needed. The reflected radiance factor β_R, is the ratio of the radiance of the sample to the radiance of the PRD, illuminated and viewed at identical geometries and with λ equal to μ. Reflected radiance factor is equal to BRF, defined in Eq. (3), if the viewing solid angle approaches zero [22]. The bispectral luminescent radiance factor $\beta_{L\lambda}$ is radiance per unit bandwidth of emission at wavelength λ when irradiated at wavelength μ divided by the radiance of a PRD, illuminated and viewed at identical geometries. The material's appearance is then presented as the Donaldson matrix [53], where β_R and $\beta_{L\lambda}$ values are tabulated as a function of excitation wavelengths μ (usually vertical) and emission wavelengths λ (usually horizontal) [53]. The β_R are the diagonal elements and the $\beta_{L\lambda}$ are the off-diagonal elements.

Generally, the emission of luminescence is assumed to be Lambertian, and the Donaldson matrix is quantified through measurements at fixed geometry conditions at one of the CIE (*Commission Internationale de l'Eclairage*) recommended geometries for colorimetry [2] e.g. 0°:45° or 45°:0°. In the following chapters and publications III and IV, goniometrical measurements of luminescence are discussed, which provide more information about appearance of the materials under study.

3.2 Characterisation of the goniofluorometer

The MIKES-Aalto goniofluorometer, originally described in [21], is designed for angularly resolved measurements of β_R and $\beta_{L\lambda}$ by employing the two-monochromator method [17]. Within the scope of this thesis, the setup has been improved by changing the beam guiding optics, resulting in increased irradiance on the sample. In addition, the setup has undergone extensive characterisation, resulting in reduced uncertainties in measuring $\beta_{L\lambda}$ as compared to [19]. The characterisation and the new uncertainty budget are described in detail in Publication III. The following sections explain the largest reductions in the uncertainties resulting from stray-light correction and characterisation of the spectral dispersion of the diffraction grating in the emission monochromator.

3.2.1 Stray-light correction

Stray light is generally an unwanted phenomenon in spectrophotometric measurements. Stray light can arise from the imperfections of the gratings used in monochromators, that cause the monochromator to transmit some light outside the desired spectral band as described in [54]. In addition, the stray light from beam guiding optics can create additional scatter around the main illuminating beam as described in [33]. Furthermore, the reflected light from the sample can be scattered within the emission monochromator as discussed below.

The measured signal on the array detector from a luminescent sample irradiated with monochromatic light, has a reflected component at wavelength μ and a luminescent component. The peak value of reflected component is generally a few orders of magnitude larger than the peak value of the luminescent component. The reflected component can be scattered within the emission monochromator and causes secondary peaks to appear in the emission spectrum as a function of emission and excitation wavelengths as shown in Figure 17.

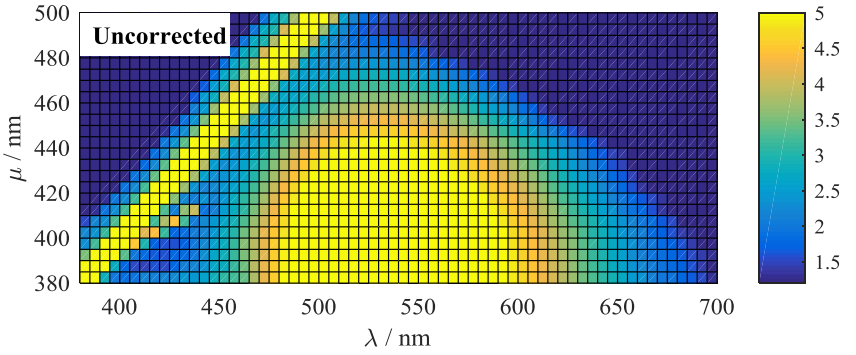

Figure 17. Uncorrected signal on the array detector of the goniofluorometer. The colour indicates the natural logarithm of the measured signal on the detector. The separation of gridlines is 5 nm.

The scattered peaks can be in the order of magnitude of the luminescence signal on the detector. In order to correct for these effects, the emission spectrum of a non-fluorescent sample – the stray-light spectrum - as a function of emission and excitation wavelengths has been measured as seen in Figure 18.

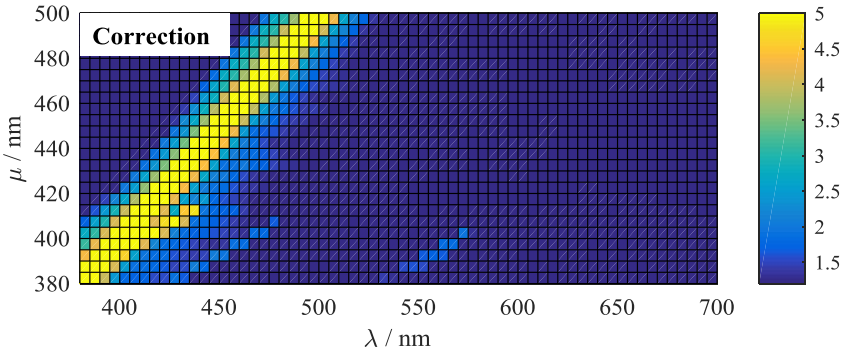

Figure 18. Correction spectrum measured from a non-luminescent sample. The colour indicates the natural logarithm of the measured signal on the detector. The separation of gridlines is 5 nm.

The stray-light spectrum is scaled so that the height of the reflected peak of the stray-light spectrum matches the height of the reflected peak in the measured spectrum of the luminescent sample. Thereafter the scaled stray-light spectrum is subtracted from the luminescence spectrum. The corrected spectrum is shown in Figure 19. In addition, the dark signal on the array detector is measured after every signal measurement and subtracted before writing the raw data to file.

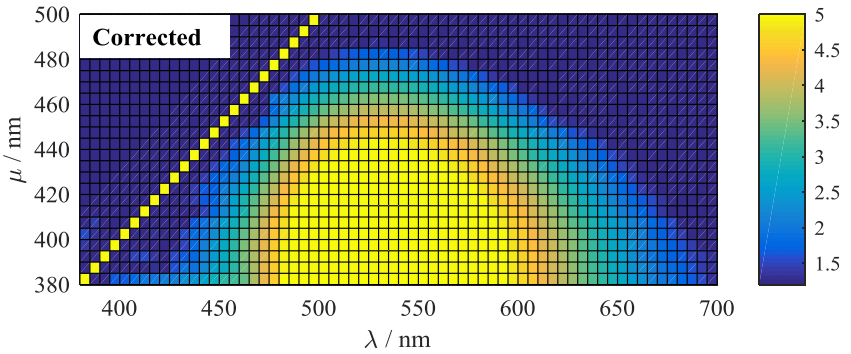

Figure 19. Corrected signal on the array detector of the goniofluorometer. The colour indicates the natural logarithm of the measured signal on the detector. The separation of gridlines is 5 nm.

The correction procedure removes the anomalous features seen in Figures 17 and 18. The remaining uncertainty component after the correction caused by the stray light and the dark signal is estimated from the standard deviation of the repeat measurements of the stray-light spectrum and is 0.20%.

3.2.2 Spectral dispersion of the detection system

The array detector of the emission monochromator of the goniofluorometer is used to measure a spectrum of 50 nm in a single image. In order to record the luminescence spectrum in the visible wavelength range, several measurements are needed with central wavelength settings 50 nm apart. Thereafter the individual 50 nm spectra are combined. Accurate processing of the spectra requires knowledge of the position of the central wavelength in the numerical index of the array detector and knowledge of the spectrally dependent dispersion of the grating in order to find the overlapping area of two consecutive spectra.

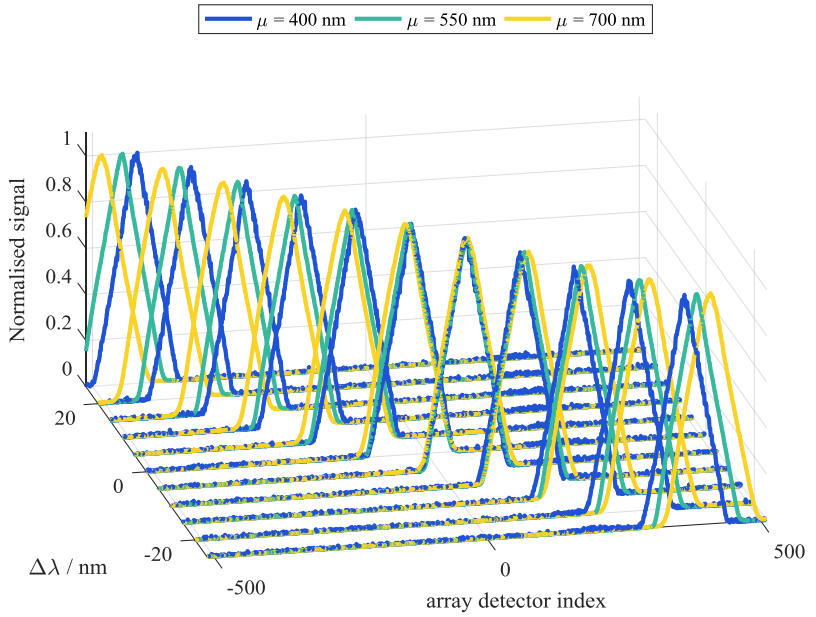

Figure 20. Observed locations of a 5 nm bandwidth spectral line at wavelength μ as the emission wavelength is set to $\lambda = \mu + \Delta\lambda$. The shifts in the array detector index are used to calculate the spectral dispersion of the grating.

In order to characterise the spectral dispersion of the grating, the excitation monochromator is set to wavelength μ and the emission monochromator is set to wavelength $\lambda = \mu + \Delta\lambda$, where $\Delta\lambda$ is from -25 nm to 25 nm with 5 nm steps. The resulting

spectra are recorded and visualised in Figure 20. It can be seen, that shifts seen in the array detector index as the wavelength λ is changed, are larger for excitation wavelength setting of μ = 700 nm than for μ = 400 nm. These shifts for the peak location in the array detector index are used to calculate the spectral dispersion of the grating. The uncertainty is evaluated by the standard deviation of several calculated spectral dispersion values and it is on the average 0.62%.

3.2.3 Validation through measurements of quantum efficiency

Quantum efficiency of the luminescence process is defined as the ratio of number of photons emitted to number of photons incident [17]. Quantum efficiency can be calculated from the goniometrically measured $\beta_{L\lambda}(\mu,\theta_v)$, as is shown in Publication III, by integrating over the VZAs θ_v and emission wavelengths λ as

$$\eta_L(\mu) = \frac{1}{\mu} \int_{\lambda_1}^{\lambda_2} \lambda \int_0^{\pi/2} \sin(2\theta_v)\beta_{L\lambda}(\mu,\theta_v) d\theta_v d\lambda \,. \tag{8}$$

This equation assumes that luminescence emission is independent of the viewing azimuth angle.

The setup and the method of goniometrical measurements of quantum efficiency have been validated against a PTFE based luminescent diffuse reflectance reference material, previously calibrated with the spectrofluorimeter at NRC [55]. The NRC provided values are calculated at fixed geometry conditions with the sample illuminated at 45° and viewed at 0°. The quantum efficiencies at MIKES are measured with 0° illumination and 15° to 85° viewing angles. The comparison results together with other values can be seen in Figure 21. It can be seen that the values measured at NRC and MIKES agree within the corresponding expanded uncertainties.

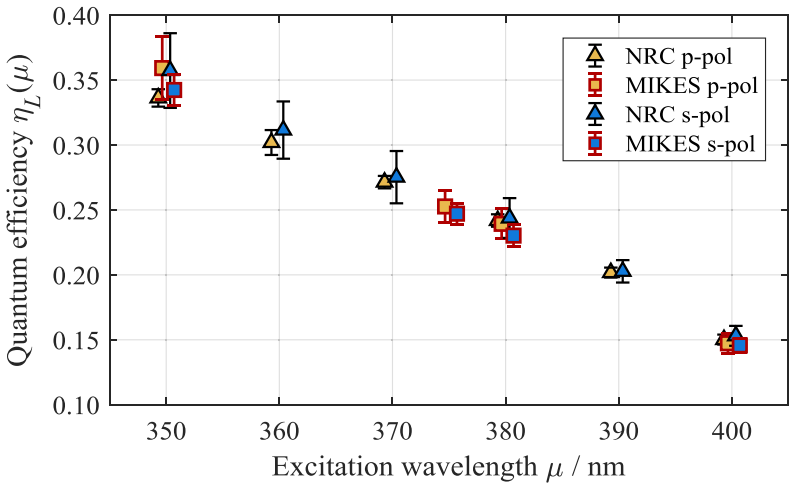

Figure 21. Spectral quantum efficiency of a PTFE based luminescent material.

3.3 Lambertian emission and reflectance of luminophores in a thin layer

The angular emission of luminescence from solid amorphous materials deviates from Lambertian as was shown in [19,20] and further confirmed in Publications II and III. The reason for the non-Lambertian emission is dependent on the material that the luminophores are bound in, rather than the phenomenon of luminescence itself.

Sintered and pressed PTFE based materials with luminophores included in the bulk are commonly used as reference samples in industries using luminescent dyes. PTFE is a translucent material or a volume reflector, which means that the incident light enters the material and is scattered many times before exiting. These volume scattering effects cause the angular distribution of reflected light to deviate from Lambertian as was shown for the PTFE based material in Figure 8. Moreover, it was shown in Publication IV that the angular distribution of reflected light from luminescent PTFE based samples depends on the absorbance of the sample. This was confirmed by modelling in the appendix of Publication IV and explained by the effective depth of the absorption process in the sample – higher absorbance values are connected to shallower absorption, which in turn are connected to more Lambertian reflectance. Similar conclusions were made in [56] by modelling and then proved by measurements of angular reflectance of paper based samples in [57].

Similar volume scattering effects happen with luminescence, with the exception that the photons emitted by the luminescence process have an isotropic angular distribution to begin with, as visualised in Figure 22 on the left. In addition, the emitted light from a luminescent sample is absorbed less by the sample, and thus has

an angular distribution that is different from that of reflectance as can be seen by comparing the top and bottom parts of Figure 23.

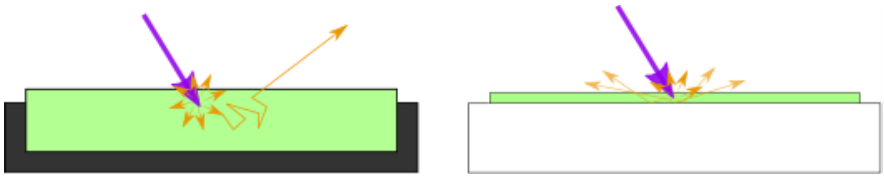

Figure 22. Volume luminescence (left) and surface luminescence (right).

One solution in achieving improved Lambertian emission and reflectance from a surface is confining the luminophores in a thin layer on a highly reflecting surface as is visualised in Figure 22 on the right. This kind of sample has been manufactured by coating a diffusely reflecting ceramic panel with a thin layer containing luminophores, binding material and a protective layer. This way, the emission takes place in a thin layer on top of the ceramic panel. The photons that are emitted towards the lower hemisphere get scattered by the ceramic surface and then by the luminescent layer and exit the material. The resulting angular emission and reflectance profiles of this ceramic sample compared to a conventional PTFE based sample can be seen in Figure 23. It can be seen that the new ceramic panel shows more Lambertian behaviour for both reflectance and luminescence than the PTFE based sample.

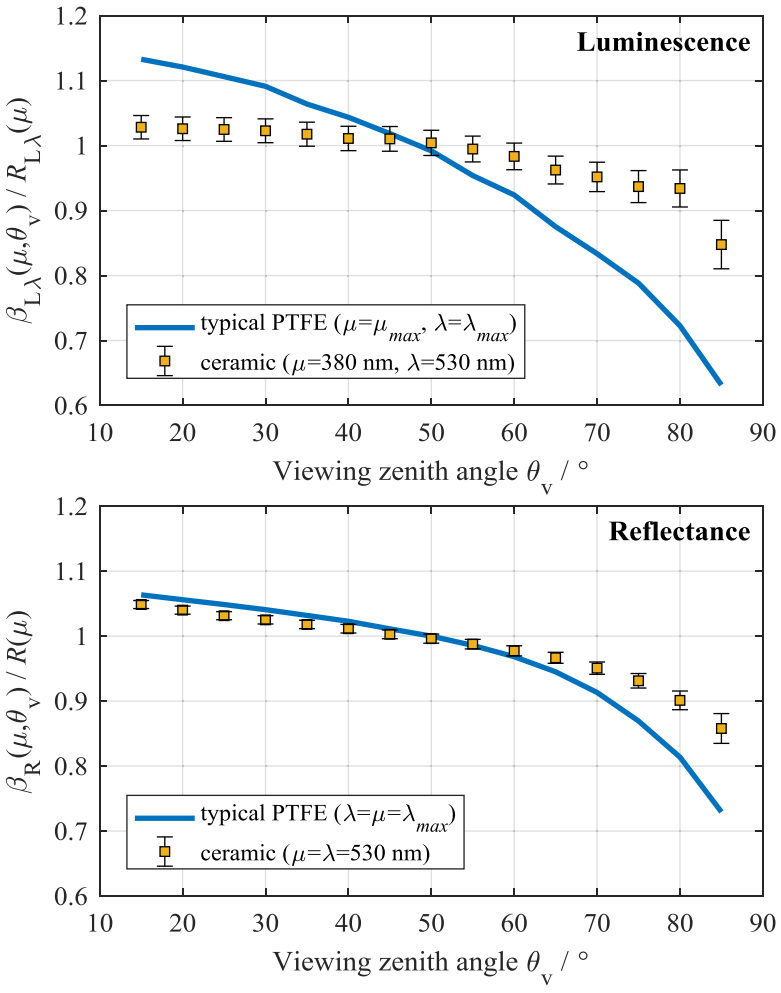

Figure 23. Normalised bispectral luminescent radiance factors (top) and reflected radiance factors (bottom) for a typical PTFE based sample and the new ceramic panel. The measurements are conducted with illumination zenith angle of 0°.

4. Conclusions

This thesis covers high accuracy angle-resolved measurements of diffuse reflectance and luminescence. The angle-resolved measurements of diffuse reflectance are used to provide SI-traceability to radiative transfer models used in Earth observation. The angle-resolved measurements of luminescence are used to improve the Lambertian reflectance and luminescence properties of reference materials used in appearance measurements of luminescent materials.

In publications I and II, progress was made towards SI-traceability of radiative transfer models by using artificial targets. In the first stage of this work the MIKES-Aalto gonioreflectometer was used to measure the BRDF of roughened surfaces of cubes made of anodised and non-anodised aluminium. The geometric errors in the BRDF measurements related to errors in sample positioning, which are usually not analysed in literature, were estimated. The measurement results were used to test two micro-facet scattering models and to develop a parameter retrieval algorithm making use of the measured polarised BRDF values. In addition, the suitability to use these surfaces in an artificial target was evaluated. In a later stage, a structured target consisting of a matrix of small cubes was made out of non-anodised aluminium and characterised for geometry and optical properties at micro scale. The measured geometry and the optical properties were used to simulate the macro scale reflectance of the target with a radiative transfer model. The modelled results were compared to macro-scale laboratory measured results and found to agree within corresponding expanded uncertainties for most of the measured geometries, but not all. It was concluded that better comparison results could be achieved by improving the processes of producing the targets, and by improved measurements of surface roughness.

In publications III and IV, progress was made in the accuracy of appearance measurements of luminescent surfaces. The earlier developed MIKES-Aalto goniofluorometer was extensively characterised to improve the accuracy of bispectral luminescent radiance factor measurements. In addition, a method for goniometrical measurements of quantum efficiency and quantum yield was validated against interlaboratory measurements. The improved measurement capability was used to describe absorbance dependent reflectance angular profiles in solid amorphous luminescent materials. In addition, most importantly, a reference material for luminescence measurements was proposed and characterised. The new material showed more Lambertian angular luminescence emission and reflectance profiles than the conventionally used PTFE based materials.

References

[1] T. A. Germer, J. C. Zwinkels, and B. K. Tsai, “Introduction,” in *Spectrophotometry: Accurate Measurement of Optical Properties of Materials*, T. A. Germer, J. C. Zwinkels, and B. K. Tsai, Eds. Amsterdam, The Netherlands: Elsevier Science, 2014, pp. 1–9.

[2] CIE 015:2004, *Colorimetry*. Commission Internationale de l’Eclairage, Vienna, Austria, 2004.

[3] C. Strothkämper, K.-O. Hauer, and A. Höpe, “How to efficiently characterize special effect coatings,” *J. Opt. Soc. Am. A*, vol. 33, no. 1, p. 1-8, 2016.

[4] H. Husu, T. Saastamoinen, J. Laukkanen, S. Siitonen, J. Turunen, and A. Lassila, “Scatterometer for characterization of diffractive optical elements,” *Meas. Sci. Technol.*, vol. 25, no. 4, 44019, p. 1-8, 2014.

[5] A. Lamminpää, S. Nevas, F. Manoocheri, and E. Ikonen, “Characterization of thin films based on reflectance and transmittance measurements at oblique angles of incidence.,” *Appl. Opt.*, vol. 45, no. 7, pp. 1392–6, 2006.

[6] S. Pourjamal, H. Mäntynen, P. Jaanson, D. Rosu, A. Hertwig, F. Manoocheri, and E. Ikonen, “Characterization of thin-film thickness,” *Metrologia*, vol. 51, no. 6, pp. S302–8, 2014.

[7] S. Y. Kotchenova, E. F. Vermote, R. Matarrese, and F. J. Klemm Jr., “Validation of a vector version of the 6S radiative transer code for atmospheric correction of satellite data. Part I: Path Radiance.,” *Appl. Opt.*, vol. 45, no. 26, pp. 6726–74, 2006.

[8] C. Justice, E. Vermote, J. Townshend, R. Defries, D. Roy, D. Hall, V. Salomonson, J. Privette, G. Riggs, A. Strahler, W. Lucht, R. Myneni, Y. Knyazikhin, S. Running, R. Nemani, Z. Wan, A. Huete, W. Leeuwen, R. Wolfe, L. Giglio, J. Muller, P. Lewis, and M. Barnsley, “The Moderate Resolution Imaging Spectroradiometer (MODIS): land remote sensing for global change research,” *IEEE Trans. Geosci. Remote Sens.*, vol. 36, no. 4, pp. 1228–49, 1998.

[9] A. Kuusk, J. Kuusk, and M. Lang, “A dataset for the validation of reflectance models,” *Remote Sens. Environ.*, vol. 113, no. 5, pp. 889–92, 2009.

[10] J. Widlowski, M. Robustelli, M. Disney, J. Gastellu-Etchegorry, T. Lavergne, P. Lewis, P. North, B. Pinty, R. Thompson, and M. Verstraete, “The RAMI On-line Model Checker (ROMC): A web-based benchmarking facility for

canopy reflectance models," *Remote Sens. Environ.*, vol. 112, no. 3, pp. 1144–50, 2008.

[11] J. Widlowski, M. Taberner, B. Pinty, V. Bruniquel-Pinel, M. Disney, R. Fernandes, J. Gastellu-Etchegorry, N. Gobron, A. Kuusk, T. Lavergne, S. Leblanc, P. E. Lewis, E. Martin, M. Mõttus, P. North, W. Qin, M. Robustelli, N. Rochdi, R. Ruiloba, C. Soler, R. Thompson, W. Verhoef, M. Verstraete, and D. Xie, "Third Radiation Transfer Model Intercomparison (RAMI) exercise: Documenting progress in canopy reflectance models," *J. Geophys. Res. Atmos.*, vol. 112, no. 9, pp. 1–28, 2007.

[12] Y. M. Govaerts and M. M. Verstraete, "Raytran: a Monte Carlo ray-tracing model to compute light scattering in three-dimensional heterogeneous media," *IEEE Trans. Geosci. Remote Sens.*, vol. 36, no. 2, pp. 493–505, 1998.

[13] J. F. W. Herschel, "On a Case of Superficial Colour Presented by a Homogeneous Liquid Internally Colourless," *Philos. Trans. R. Soc. London*, vol. 135, pp. 143–5, 1845.

[14] U. Resch-Genger, K. Hoffmann, W. Nietfeld, A. Engel, J. Neukammer, R. Nitschke, B. Ebert, and R.Macdonald, "How to improve quality assurance in fluorometry: fluorescence-inherent sources of error and suited fluorescence standards.," *J. Fluoresc.*, vol. 15, no. 3, pp. 337–62, 2005.

[15] L. Möckl, D. C. Lamb, and C. Bräuchle, "Super-resolved Fluorescence Microscopy: Nobel Prize in Chemistry 2014 for Eric Betzig, Stefan Hell, and William E. Moerner.," *Angew. Chem. Int. Ed. Engl.*, pp. 2–8, 2014.

[16] ISO 11475:2004, *Paper and board - Determination of CIE whiteness, D65/10 degrees (outdoor daylight)*. International Organization for Standardization, Geneva, Switzerland, 2004.

[17] CIE 182:2007, *Calibration Methods and Photoluminescent Standards for Total Radiance Factor Measurements*. Commission Internationale de l'Eclairage,Vienna, Austria, 2007.

[18] I. H. Lambert, *Photometria sive de mensura et gradibus luminis, colorum et umbrae*. sumptibus viduae Eberhardi Klett, 1760.

[19] S. Holopainen, F. Manoocheri, and E. Ikonen, "Non-Lambertian behaviour of fluorescence emission from solid amorphous material," *Metrologia*, vol. 46, no. 4, pp. S197–1, 2009.

[20] B. Bernad, A. Ferrero, A. Pons, M. L. Hernanz, and J. Campos, "Upgrade of goniospectrophtometer GEFE for near-field scattering and fluorescence

radiance measurements," in *Proc. of SPIE-IS&T*, 2015, vol. 9398, 93980E, pp. 1-10.

[21] S. Holopainen, F. Manoocheri, and E. Ikonen, "Goniofluorometer for characterization of fluorescent materials," *Appl. Opt.*, vol. 47, no. 6, pp. 835–42, 2008.

[22] F. E. Nicodemus, J. C. Richmond, J. J. Hsia, I. Ginsberg, and T. Limperis, *Geometrical considerations and nomenclature for reflectance*. National Bureau of Standards (US), Washington D.C., USA, 1977.

[23] G. Obein, R. Bousquet, and M. E. Nadal, "New NIST reference goniospectrometer," in *Proc. SPIE 5880, Optical Diagnostics*, 2005, 58800T, pp. 1-10.

[24] T. A. Germer, J. C. Stover, and S. Schröder, "Angle-resolved diffuse reflectance and transmittance," in *Spectrophotometry: Accurate Measurement of Optical Properties of Materials*, T. A. Germer, J. C. Zwinkels, and B. K. Tsai, Eds. Amsterdam, The Netherlands: Elsevier Science, 2014, pp. 291–328.

[25] T. A. Germer, J. C. Zwinkels, and B. K. Tsai, "Theoretical concepts in spectrophotometric measurements," in *Spectrophotometry: Accurate Measurement of Optical Properties of Materials*, T. A. Germer, J. C. Zwinkels, and B. K. Tsai, Eds. Amsterdam, The Netherlands: Elsevier Science, Amsterdam, The Netherlands, 2014, pp. 11–66.

[26] M. Born and E. Wolf, *Principles of Optics*, 7th ed. Cambridge University Press, New York, USA, 2011.

[27] CIE S 017/E:2011, *ILV: International Lighting Vocabulary*. Commission Internationale de l'Eclairage, Vienna, Austria, 2011.

[28] A. Höpe, T. Atamas, D. Hünerhoff, S. Teichert, and K.-O. Hauer, "ARGon3: '3D appearance robot-based gonioreflectometer' at PTB.," *Rev. Sci. Instrum.*, vol. 83, no. 4, 45102, pp. 1-8, 2012.

[29] S. Nevas, F. Manoocheri, and E. Ikonen, "Gonioreflectometer for measuring spectral diffuse reflectance," *Appl. Opt.*, vol. 43, no. 35, pp. 6391–9, 2004.

[30] A. Höpe, A. Koo, F. Verdu, F. Leloup, G. Obein, G. Wübbeler, J. Campos, P. Iacomussi, P. Jaanson, S. Källberg, M. Šmíd, "'Multidimensional reflectometry for industry' (xD-Reflect) an European research project," in *Proc. of SPIE-IS&T*, 2014, vol. 9018, 901804, pp. 1-11.

[31] N. Fox, E. Woolliams, J. Widlowski, J. Hollandt, M. Rajteri, J. Dubard, A.

Lassila, F. Manoocheri, W. Finsterle, F. Olschewski, R. Reulke, E. Honkavaara, and P. Preusse, “Metrology for Earth observation and climate 1 (MetEOC),” in *Proceedings of NEWRAD 2014*, 2014, pp. 67–8, http://newrad2014.aalto.fi/.

[32] C. Strothkämper, A. Ferrero, A. Koo, P. Jaanson, G. Ged, G. Obein, S. Källberg, J. Audenaert, F. Leloup, F. Marínez-Verdú, E. Perales, A. Schirmacher, and J. Campos, “Multilateral spectral radiance factor scale comparison,” *Appl. Opt.*, vol. 56, no. 7, pp. 1996–2006, 2017.

[33] S. Holopainen, F. Manoocheri, S. Nevas, and E. Ikonen, “Effect of light scattering from source optics in goniometric diffuse reflectance measurements,” *Metrologia*, vol. 44, no. 3, pp. 167–70, 2007.

[34] M. Kivi, “Sample Alignment for Diffuse Reflectance Measurements,” MSc thesis, Aalto University School of Electrical Engineering, 2014.

[35] A. D. Rakić, “Algorithm for the determination of intrinsic optical constants of metal films: application to aluminum.,” *Appl. Opt.*, vol. 34, no. 22, pp. 4755–67, 1995.

[36] M. R. Querry, *Optical Constants*. Missoury University, Kansas City, USA, Technical report ADA158623, 1985.

[37] N. Oreskes, K. Shrader-Frechette, and K. Belitz, “Verification, Validation, and Confirmation of Numerical Models in the Earth Sciences,” *Science*, vol. 263, no. 5147, pp. 641–6, 1994.

[38] B. T. Phong, “Illumination for Computer Generated Pictures,” *Commun. ACM*, vol. 18, no. 6, pp. 311–7, 1975.

[39] S. D. Butler, S. E. Nauyoks, and M. A. Marciniak, “Comparison of microfacet BRDF model to modified Beckmann-Kirchhoff BRDF model for rough and smooth surfaces,” *Opt. Express*, vol. 23, no. 22, 29100, pp. 1-13, 2015.

[40] Y. Sun, “Statistical ray method for deriving reflection models of rough surfaces.,” *J. Opt. Soc. Am. A. Opt. Image Sci. Vis.*, vol. 24, no. 3, pp. 724–44, 2007.

[41] E. M. Sparrow, K. E. Torrance, and R. C. Birkebak, “Theory for Off-Specular Reflection From Roughened Surfaces,” *J. Opt. Soc. Am.*, vol. 57, no. 9, pp. 1105–14, 1967.

[42] M. W. Hyde, J. D. Schmidt, and M. J. Havrilla, “A geometrical optics polarimetric bidirectional reflectance distribution function for dielectric and metallic surfaces,” *Opt. Express*, vol. 17, no. 24, pp. 22138–53, 2009.

[43] R. G. Priest, “Polarimetric microfacet scattering theory with applications to absorptive and reflective surfaces,” *Opt. Eng.*, vol. 41, no. 5, pp. 988-93, 2002.

[44] R. Cook and K. Torrance, “A reflectance model for computer graphics,” *ACM Trans. Graph.*, vol. 1, no. 1, pp. 7–24, 1982.

[45] M. Bass, J. M. Enoch, E. W. Stryland, and W. L. Wolfe, Eds., *Handbook of Optics*, 2nd ed., vol. 1. McGraw-Hill, Inc., USA, 1995.

[46] J. F. Blinn, “Models of light reflection for computer synthesized pictures,” *ACM SIGGRAPH Comput. Graph.*, vol. 11, no. 2, pp. 192–8, 1977.

[47] J. Renders and S. Flasse, “Hybrid methods using genetic algorithms for global optimization,” *IEEE Trans. Syst. MAN, Cybern. B Cybern.*, vol. 26, no. 2, pp. 243–58, 1996.

[48] T. Takatsuji, T. Eom, A. Tonmueanwai,R. Yin, F. van der Walt, S. Gao, B. Thu, R. Singhal, E. Howick, K. Doytchinov, J. Valente de Oliveira, A. Lassila, J. O'Donnell, and A. Balsamo, “Final report on APMP regional key comparison APMP.L-K6: Calibration of ball plate and hole plate,” *Metrologia*, vol. 51, no. 1A, p. 4003, 2014.

[49] J. Zwinkels, P. C. DeRose, and J. E. Leland, “Spectral Fluorescence Measurements,” in *Spectrophotometry: Accurate Measurement of Optical Properties of Materials*, T. A. Germer, J. C. Zwinkels, and B. K. Tsai, Eds. Elsevier, 2014, pp. 221–90.

[50] J. R. Lakowicz, “Introduction to Fluorescence,” in *Principles of Fluorescence Spectroscopy*, Springer US, Boston, USA, 2006, pp. 1–25.

[51] Labsphere Inc., “Fluorescence Materials.” Labsphere Inc., North Sutton, NH, USA, 2015.

[52] L. Yang, “Detailed analysis of the UV-adjustment techniques used in paper and graphic industries,” *Color Res. Appl.*, vol. 42, no. 1, pp. 19–26, 2017.

[53] R. Donaldson, “Spectrophotometry of fluorescent pigments,” *Br. J. Appl. Phys.*, vol. 5, no. 6, pp. 210–4, 1954.

[54] M. H. Sharpe and Irish D., “Stray Light in Diffraction Grating Monochromators,” *Opt. Acta Int. J. Opt.*, vol. 25, no. 9, pp. 861–93, 1978.

[55] J. C. Zwinkels, “Instrumentation, standards, and procedures used at the National Research Council of Canada for high-accuracy fluorescence measurements,” *Anal. Chim. Acta*, vol. 380, no. 2–3, pp. 193–209, 1999.

[56] M. Neuman and P. Edström, “Anisotropic reflectance from turbid media. I. Theory.,” *J. Opt. Soc. Am. A. Opt. Image Sci. Vis.*, vol. 27, no. 5, pp. 1032–9, 2010.

[57] M. Neuman and P. Edström, “Anisotropic reflectance from turbid media. II. Measurements.,” *J. Opt. Soc. Am. A. Opt. Image Sci. Vis.*, vol. 27, no. 5, pp. 1040–5, 2010.

Publication I

P. Jaanson, F. Manoocheri, H. Mäntynen, M. Gergely, J.-L. Widlowski, and E. Ikonen, “Gonioreflectometric properties of metal surfaces,” *Metrologia*, vol. 51, no. 6, pp. S314–S318, Dec. 2014.

Publication II

P. Jaanson, A. Bialek, C. Greenwell, H. Mäntynen, J-L. Widlowski, F. Manoocheri, A. Lassila, N. Fox, and E. Ikonen, “Towards SI-traceability of a Monte Carlo radiative transfer model in the visible range,” *IEEE Trans. Geosci. Remote Sens.* (accepted for publication).

Publication III

P. Jaanson, F. Manoocheri, and E. Ikonen, “Goniometrical measurements of fluorescence quantum efficiency,” *Meas. Sci. Technol.*, vol. 27, no. 2, 25204, pp. 1-8, 2016.

Publication IV

P. Jaanson, T. Pulli, F. Manoocheri, and E. Ikonen, “A reference material with close to Lambertian reflectance and fluorescence emission profiles,” *Metrologia*, vol. 53, no. 6, pp. 1330–1338, 2016.

Aalto-DD 195/2017
VTT SCIENCE 164

ISBN 978-952-60-7657-7 (printed)
ISBN 978-952-60-7656-0 (pdf)
ISSN-L 1799-4934
ISSN 1799-4934 (printed)
ISSN 1799-4942 (pdf)

978-951-38-8575-5 (printed)
978-951-38-8574-8 (pdf)
2242-119X
2242-119X (printed)
2242-1203 (pdf)

Aalto University
School of Electrical Engineering
Metrology Research Institute
www.aalto.fi

BUSINESS +
ECONOMY

ART +
DESIGN +
ARCHITECTURE

SCIENCE +
TECHNOLOGY

CROSSOVER

**DOCTORAL
DISSERTATIONS**